Development of a Mouse Pain Scale Using Sub-second Behavioral Mapping and Statistical Modeling

Ishmail Abdus-Saboor[1,2,7], **Nathan T. Fried**[1,6,7], **Mark Lay**[3], **Justin Burdge**[1,2], **Kathryn Swanson**[4], **Roman Fischer**[4], **Jessica Jones**[2], **Peter Dong**[1], **Weihua Cai**[5], **Xinying Guo**[5], **Yuan-Xiang Tao**[5], **John Bethea**[4], **Minghong Ma**[1], **Xinzhong Dong**[3], **Long Ding**[1], **Wenqin Luo**[1,8,*]

[1]Department of Neuroscience, Perelman School of Medicine, University of Pennsylvania, Philadelphia, PA 19104, USA

[2]Department of Biology, School of Arts and Sciences, University of Pennsylvania, Philadelphia, PA 19104, USA

[3]Howard Hughes Medical Institute and Department of Neuroscience, Johns Hopkins University, School of Medicine, Baltimore, MD 21205, USA

[4]Department of Biology, Drexel University, College of Arts and Sciences, Philadelphia, PA 19104, USA

[5]Department of Anesthesiology, Rutgers University Medical School, Newark, NJ 07101, USA

[6]Department of Biology, Rutgers University, Camden, NJ 08102, USA

[7]These authors contributed equally

[8]Lead Contact

SUMMARY

Rodents are the main model systems for pain research, but determining their pain state is challenging. To develop an objective method to assess pain sensation in mice, we adopt high-speed videography to capture sub-second behavioral features following hind paw stimulation with both noxious and innocuous stimuli and identify several differentiating parameters indicating the affective and reflexive aspects of nociception. Using statistical modeling and machine learning, we integrate these parameters into a single index and create a "mouse pain scale," which allows us to assess pain sensation in a graded manner for each withdrawal. We demonstrate the utility of this method by determining sensations triggered by three different von Frey hairs and optogenetic

*Correspondence: luow@pennmedicine.upenn.edu.

activation of two different nociceptor populations. Our behavior-based "pain scale" approach will help improve the rigor and reproducibility of using withdrawal reflex assays to assess pain sensation in mice.

Graphical Abstract
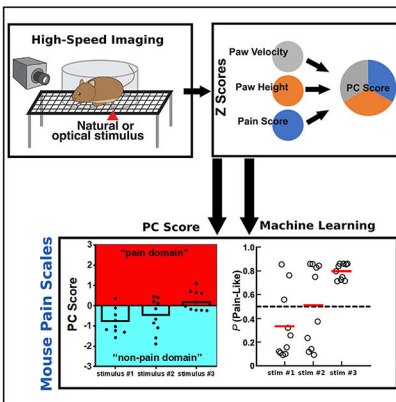
In Brief

Abdus-Saboor et al. develop a behavior-centered "mouse pain scale" using high-speed videography, statistical modeling, and machine learning. With this method, they assess the sensation induced by noxious, innocuous, and optogenetic stimuli. This method will improve the reliability of using the mouse hind paw withdrawal to measure pain.

INTRODUCTION

Chronic pain affects more than 25 million people in the United States, yet the underlying mechanisms are still not fully understood. Pain is a complicated and subjective experience, which is challenging for objective assessment. In humans, pain assessment relies on the patient's own description of his or her pain experience, which is roughly quantified by self-assignment along a single-score pain scale. To investigate the mechanisms responsible for chronic pain, it is imperative to use animal models, such as rodents. However, it is equally, if not more, difficult to objectively measure pain sensation in rodents because they are non-verbal. Researchers have relied on behaviors to infer their pain state, but many in the field have recently raised the question of whether these assays are truly reflective of pain sensation in the animal (Deuis et al., 2017).

The current behavior assays to assess pain sensation in rodents can be broadly classified as operant pain assays, spontaneous pain detection assays, and reflexive withdrawal assays (Barrot, 2012; Le Bars et al., 2001; Mogil, 2009; Yuan et al., 2016). Operant assays typically involve animals' successfully completing a task or learning to avoid or prefer a chamber that is associated with pro- or anti-nociceptive stimuli or experiences (Hung et al., 2015; Mauderli et al., 2000; Nag and Mokha, 2016; Rohrs et al., 2015). Because these assays require normal learning and memory processes for the animal to report its preference or avoidance, the failure of an animal to learn or remember a pro-nociceptive chamber or task

may not necessarily indicate a lack of pain. Spontaneous pain detection assays, such as the grimace scale or paw licking and biting, have the advantage of mimicking the spontaneous pain that is commonly observed in the clinic (Langford et al., 2010; Tuttle et al., 2018). Nevertheless, the grimace scale does not work well with neuropathic pain models, with the exception of the chronic constriction injury model in the trigeminal area (Akintola et al., 2017).

Over the past 50 years, the most widely used measurements of pain sensation in rodents are reflexive withdrawal assays, in which a stimulus is applied to a region of the rodent, such as the paw or tail, and the withdrawal frequency is quantified as a readout for the animal's pain state (Barrot, 2012; Le Bars et al., 2001; Yuan et al., 2016). Obvious advantages to reflexive assays are the ease of the procedures, the ability to test many animals in a short time period, and the similarities to human reflexes that allow the interpretation of the results on the basis of the human experience. Although these assays have led to many important discoveries, they also have some well-recognized drawbacks. First, there is not always a linear relationship between stimulus intensity and the frequency of withdrawal reflex, as a high frequency of paw withdrawal is observed for both noxious pinprick and innocuous dynamic brush (DB) (Cui et al., 2016; Duan et al., 2014). To interpret the results, the experimenters must define a given stimulus as noxious or innocuous, such that noxious stimuli trigger "pain" withdrawal reflex, whereas innocuous stimuli trigger "non-pain" withdrawal reflex. However, because the definitions of noxious and innocuous stimuli rely on subjective human judgment, it will generate inconsistency when different research groups cannot reach a consensus on the quality of a stimulus. For example, despite the popularity of the von Frey hair (VFH) test, there is no consensus on the sensation that is triggered by VFHs in rodents (Bove, 2006; Bradman et al., 2015; Lambert et al., 2009). In addition, humans and rodents may have a different sensory experience to a given stimulus (i.e., a stimulus that is innocuous to humans could be noxious to rodents), so the human sensory experience may not be reliable for annotating the quality of a stimulus when it is applied to a rodent.

Inspired by the application of high-speed videography in the fly, fish, and mouse to map movement features of specific behaviors (Browne et al., 2017; Kim et al., 2017; Muijres et al., 2014; Wolman et al., 2011), we reasoned that this high-speed imaging method could help quantify mouse pain sensation in a more objective and unbiased manner. Recently, other groups have used high-speed imaging to study rodent behaviors triggered by either noxious pinprick or optogenetic activation of all nociceptors (Blivis et al., 2017; Browne et al., 2017). Nevertheless, these previous studies did not examine behaviors in response to innocuous stimuli, so how to distinguish "pain" versus "non-pain" behaviors remains uncertain.

In this study, we adopted high-speed imaging to capture movement features of the mouse paw withdrawal reflex in response to a set of noxious and innocuous natural mechanical stimuli. Prior to performing high-speed behavioral analysis, we used whole-animal *in vivo* calcium imaging to confirm that cotton swab (CS) and DB mainly activated intermediate- and large-diameter dorsal root ganglion (DRG) neurons (low-threshold mechanoreceptors for triggering "touch" sensation), whereas pinprick preferentially activated small-diameter DRG neurons (high-threshold nociceptors for triggering "pain" sensation). Using these four

well-defined innocuous and noxious mechanical stimuli, we characterized sub-second paw and head movement features of the withdrawal reflex in CD1 and C57 male and female mice. We identified six distinguishing features, which indicated both reflexive and affective aspects of nociception, and combined them using principal-component analyses into a single index to map each withdrawal reflex into a graded "mouse pain scale." A threshold separating the "pain" from the "non-pain" domain was also identified. We further generated a probability prediction of being "pain-like" for each withdrawal reflex using machine learning.

As a proof of principle, we applied this method and our parameter database to study paw withdrawal in response to three VFHs and demonstrated the sensation triggered by different VFHs under baseline conditions. As a second proof of principle, we revealed that acute optical activation of a broad nociceptor population, using *Trpv1^Cre*-mediated recombination (*Trpv1-ChR2* mice), led to a characteristic "painful" paw withdrawal, whereas optical activation of a more restricted population of nociceptors, MRGPRD+ non-peptidergic nociceptors (*Mrgprd-ChR2* mice), led to a non-painful paw withdrawal under baseline conditions. Under chronic inflammation, the same optical activation of MRGPRD+ non-peptidergic nociceptors triggered "painful" paw withdrawals. "Pain-like" withdrawal reflexes of both *Trpv1-ChR2* and sensitized *Mrgprd-ChR2* mice were completely reversed to non-painful withdrawals following analgesic administration. Because *Trpv1-ChR2* and *Mrgprd-ChR2* mice show an indistinguishable high frequency (>70%) of paw withdrawal upon optical stimulation under all conditions, these results highlight the precision of our method to annotate the mouse "pain state." Taken together, our data suggest that a sensitive pain sensation assessment can be feasibly achieved on the basis of calibration to the animal's own behavior. This unified "pain scale" assessment method will help improve the rigor and reproducibility of rodent pain research.

RESULTS

In Vivo Calcium Imaging to Determine Stimulus Quality

We sought to identify sub-second behavioral features of mouse hind paw withdrawal reflex that could indicate whether a rodent was experiencing pain. We began our analysis with four natural mechanical stimuli that are widely used in the field as innocuous or noxious. They were static CS (gently pressing a blunted, cone-shaped CS against the plantar surface of the hind paw, which represents an innocuous static mechanical stimulus), DB (sweeping a soft-bristled makeup brush from the proximal to distal plantar surface, which represents an innocuous dynamic mechanical stimulus), light pinprick (LP; gently placing a needle on the plantar surface, which represents a potentially noxious mechanical stimuli), and heavy pinprick (HP; forcefully pushing a needle onto the plantar surface, which represents a noxious mechanical stimuli).

To validate these stimuli as noxious versus innocuous, we first examined the sensory neuron populations that were activated by these four stimuli with *in vivo* calcium imaging in a mouse line (Kim et al., 2016), whereby Ca^{2+} transients were recorded from ~1,500 DRG neurons per trial with the genetically encoded calcium indicator *GCAMP6* driven by the *Pirt* promoter (Figure S1). We applied each stimulus to the hind paw of lightly anesthetized Pirt-

GCAMP6 mice in an innocuous to noxious order while recording DRG Ca^{2+} influx (Figure S1A). Robust and rapid Ca^{2+} influx occurred within DRG neurons following the application of all four stimuli, and the number of activated neurons positively correlated with the stimulus intensity (Figure S1B). On average, we observed Ca^{2+} transients increasing between 1- and 4-fold over baseline following the application of stimuli (Figures S1C–S1J; Data S1). Moreover, CS and DB predominantly activated intermediate-diameter (20–25 μm) or large-diameter (>25 μm) DRG neurons, while the light and HP stimuli predominantly activated small-diameter (<20 μm) DRG neurons (Figures S1K and S1L). These activation patterns are consistent with the notion that CS and DB stimuli preferentially trigger"touch" sensation by activating large-diameter low-threshold mechanoreceptors, whereas pinprick stimuli preferentially trigger "pain" sensation by activating small-diameter high-threshold nociceptors.

High-Speed Imaging of Paw Withdrawal Reflex Revealed Distinctive Movement Features in Response to Innocuous and Noxious Mechanical Stimuli

With confirmation of the stimulus quality, we applied these four mechanical stimuli to the plantar surface of a randomly chosen hind paw of fully acclimated mice and used high-speed videography (500–1,000 fps) to record sub-second, full-body movements (Figure 1A). To test for potential genotype- and/or sex-specific features, we examined responses in male and female CD1 and C57 wild-type mice (n = 10 animals for each group). All four mechanical stimuli evoked movements of the stimulated paw, the head, and the entire body, and such movements would be completed around 500 ms (Video S1 shows representative videos from CD1 males). We found similar patterns in both male (Figure 1) and female (Figure S2) mice. A typical movement sequence involved the stimulated hind paw moving away from or the head turning toward the stimulus, followed by the whole body turning. We focused on the movement features of the paw and head because they are most closely related to the stimulus onset and thus more likely to reflect sensation evoked by the stimuli. The paw-associated movements usually started with the paw being raised to a maximum height. It would then be held at the apex, returned to the wire mesh, or begin a sinusoidal paw shake (Figure 1B). In some pinprick trials, the mouse would jump into the air with all four paws rising away from the stimulus (Figure 1C). The mouse would then return its paw to the mesh, often in a guarding manner (only toes or heel of the paw in contact with the mesh) (Figure 1D). The head-associated movements involved orientation and turning of the head toward the stimulus. In some instances, primarily with noxious pinprick stimuli, the mouse would display orbital tightening, which occurs in mice during pain-related grimace (Figure 1E; Langford et al., 2010).

For both C57 and CD1 male mice, the likelihood of observing paw and/or head movement and the temporal order between paw or head movements depended on the stimulus type (Figure 1). Paw movement occurred in 30%–40% of trials with CS for males of both genotypes, 70% in C57 and 100% in CD1 with DB, and nearly 100% for both genotypes with pinprick stimuli (Figures 1F and 1I). Head movement showed the opposite trend; it occurred in 80%–100% of CS and DB trials but only 47%–60% of light and HP trials (Figures 1L and 1M). For both genotypes, paw movement was initiated earlier than head movement in most pinprick trials, while the order was more variable for CS and DB stimuli

(Figures 1G and 1J). For DB, LP, and HP, the latency to the head response was ~50 ms for both genotypes (Figures 1H and 1K). The paw response latency was also ~50 ms for pinprick stimuli and 100 ms for DB. The latency to paw or head movement for CS was much longer, taking more than 500 ms for a response. Together, these results suggest that innocuous mechanical stimuli preferentially trigger an "exploring head turn" reflex, whereas noxious mechanical stimuli preferentially evoke a quick "avoidance paw withdrawal" reflex.

Moreover, the prevalence of certain movements, such as orbital tightening, paw shake, jumping, and paw guarding (Figures 1B–1E), are closely correlated with the stimulus quality. Their incidence is 10% and 15% in the CS and DB trials but much greater in the LP (60%) and HP (85%) trials (Figures 1L and 1M). Together, this high-speed imaging method allowed us to capture detailed kinematics of the mouse paw withdrawal reflex.

A Subset of Movement Parameters Account for the Majority of Variance in the Responses

To determine which movement features best distinguish between behaviors in response to innocuous and noxious stimuli, we measured a set of parameters for approximately half of trials with CD1 and C57 male mice as a pilot analysis, including (1) the total time the paw is in motion (total paw time), (2) the total time the paw is in the air (paw airtime), (3) the total time the paw is held at the apex (paw at apex), (4) the total time the paw is in motion after reaching the apex (paw time after apex), (5) paw lift height, (6) paw lift velocity, (7) response latency (whether it be the head or paw), (8) the duration of head movement, (9) the duration of full-body movement, (10) the total behavior time, and (11) a pain score, which is a composite measurement of orbital tightening, jumping, paw shaking, and paw guarding (e.g., animals featuring three of these four behaviors would be assigned a score of 3 for that particular trial). These 11 parameters reflect a mixture of behaviors associated with both the sensory reflexive and affective components of pain (Corder et al., 2017).

With these multi-dimensional data, we first tried to decide which of the 11 parameters accounted for the majority of variance. Total paw time, paw air time, paw at apex, and paw time after apex were highly correlated (Figure S3A), suggesting that these four parameters were redundant for measuring the same underlying effect. We then performed an iterative exploratory factor analysis with the remaining 8 parameters (Figure S3B) and found that 3 parameters (paw height, paw velocity, and pain score) had high factor loadings (Figure S3B) and featured an increasing trend in raw values with increasing stimulus intensity, indicating that they likely accounted for the majority of the system's variance and would be the most useful for differentiating between behaviors evoked by innocuous and noxious stimuli. Indeed, only these three parameters showed some significant differences between the behaviors evoked by innocuous versus noxious stimuli (Figure 2; Figures 1, S2, and S4 show the other measurements). Therefore, we subsequently used these three parameters, which encompass both reflexive (paw height and paw velocity) and affective (pain score) components of the pain response, to analyze withdrawal reflex behaviors of all mice (Figure 2).

A Combination of Distinguishing Behavioral Parameters Can Indicate Mouse Pain Sensation

Although each of the three parameters provides information that helps distinguish movements induced by noxious versus innocuous stimuli, they are expressed in different dimensions with regard to both absolute values and units. In addition, it is unclear what the exact "pain versus non-pain" threshold is for each parameter. To take advantage of the entire set of information, we sought to combine these three different parameters into a one-dimensional score using a principal-component analysis (PCA): first converting the raw data to normalized Z scores within each dataset (Figures 3A–3L) and then applying a PCA on converted Z scores to determine the relative contribution of each parameter (as reflected by eigenvalues; see Table 1). The first principal component (PC1) score of the three-dimensional dataset was computed as a weighted total value. To account for potential genotype and sex differences, the PCA was initially performed separately for the four genotype-sex combinations, generating four separate sets of eigenvalues to calculate PC scores.

With this transformation, we were able to plot the PC scores for reflex behaviors in response to each stimulus within males and females of both genotypes (Figures 3M–3P). We found that (1) different from the withdrawal frequency, mean PC scores were positively correlated with increasing stimulus intensity (i.e., PC scores for CS < DB < pinprick) in males and females of both genotypes, (2) mean PC scores for LP trials were the most variable across genotype and sex (i.e., PC scores were positive for most CD1 male trials but negative for most CD1 female trials, suggesting that LP may trigger a different sensation in male and female mice), and (3) for a given stimulus type in a given strain and sex combination, there was considerable variation in PC scores among different mice, which may be caused by variations of the internal state of each animal during testing (i.e., alert, resting, etc.) or the slight stimulus variability from trial to trial. Taken together, our PC-based analysis suggests that the PC score of each mouse can be used to map its "pain state" and intensity, essentially creating a "mouse pain scale," with a score of 0 serving as the threshold to separate pain versus non-pain domains.

Machine Learning Classifies Withdrawal Behaviors as a Probability of Being Pain-like

To further classify mouse pain sensation on the basis of their reflexive behaviors, we used a machine-learning approach to predict the probability of each trial being pain-like. Specifically, we used the PC scores of CS and HP trials from one group of mice to train a support vector machine (SVM; see STAR Methods). CS and HP trials were chosen because their triggered behaviors can be defined as "non-pain" or "pain" with high confidence and the corresponding PC scores showed the most consistent patterns across genotype and gender. The trained SVM was then used to predict the probability of being "pain-like" for all trials (Figure 4A; the code can be found at https://data.mendeley.com/datasets/mcygb8762v/1 and https://github.com/longdecision/PainAssaySVM).

We first determined the predicted pain-like probability for withdrawal reflex triggered by DB or LP within the same genotype and sex group. To do this, the SVM was trained with CS and HP data from CD1 males (Figure 4B), CD1 females (Figure 4G), C57 males (Figure

4L), or C57 females (Figure 4Q) for the genotype and sex-specific analysis (e.g., the SVM was trained with CS and HP trials of CD1 females in Figure 4G to analyze the pain-like probabilities of DB and LP trials of CD1 females in Figure 4G). The pain-like probabilities for behaviors triggered by DB ranged from 0.20 to 0.33 and for LP ranged from 0.47 to 0.65 (Figures 4B, 4G, 4L, and 4Q). Thus, these results suggest that DB had a low probability of evoking pain-like sensation (<0.33) in each sex of both genotypes, despite the ~100% responsive rate. Notably, the SVM predictions revealed that only responses of CD1 males to LP had a high probability of being pain-like (0.65). In all other groups, the probability was no greater than 0.55. Thus, similar to PC scores, these results suggest that mice with different genetic backgrounds or sex may sense LP as noxious or innocuous.

Given the known effect of genetic background and sex on pain sensation, we next asked whether an SVM trained with data from one sex and genotype could reliably classify similar trials from the other sexes and genotypes (e.g., the SVM trained with CS and HP trials of CD1 females [Figure 4G] was used to analyze the pain-like probabilities of CS, DB, LP, and HP trials of CD1 males [Figure 4F], C57 males [Figure 4H], and C57 females [Figure 4I]). Under these conditions, we found a consistently high pain-like probability for HP trials (range 0.69–0.96) and a low pain-like probability for CS trials (range 0.08–0.28). DB was also consistently predicted to have a low probability of being pain-like (range 0.14–0.39), while LP was consistently predicted to have a boundary probability of being pain-like (range 0.39–0.68). Notably, predictions for DB and LP, when trained with a different sex or genotype, are more variable than the predictions made when training with the same sex and genotype. Thus, the SVM trained with CS and HP data from one sex and genotype group could reliably classify responses to the same stimuli from another group. Classification of responses to other stimuli, such as DB or LP, may work better with training datasets from the same sex and genotype group.

Proof of Principle 1: High-Speed Imaging Analysis of Paw Withdrawal Reflex Triggered by VFHs

We next sought to demonstrate the usefulness of this approach by analyzing the paw withdrawal reflex of CD1 male mice in response to three VFHs (0.6, 1.4, and 4.0 g). These filaments are often used to measure mechanical threshold or mechanical pain responses in mice (Cheng et al., 2017). Although each VFH delivers a well-defined amount of mechanical force, whether it triggers a nociceptive or non-nociceptive response for a mouse under a given condition is uncertain.

We found that CD1 male mice responded to 50% of 0.6 g VFH trials, 90% of 1.4 g VFH trials, and 100% of 4.0 g VFH trials (Figure 5A; Video S1), similar to what is reported in the literature (Cheng et al., 2017; Duan et al., 2014). Paw height and paw velocity were significantly greater for 4.0 g VFH compared with 1.4 and 4 g VFH (p = 0.004 and p = 0.027 [height], p < 0.0001 and p = 0.012 [velocity], respectively) (Figures 5B and 5C). No statistical difference (p > 0.215) in pain score was found between any of the filaments (Figure 5D). The PC score of each response to a given VFH was calculated using the previously obtained CD1 male database (see STAR Methods). On average, PC scores were positive (0.246) for 4.0 g VFH but negative for 0.6 g (−0.957) and 1.4 g (−0.498) (Figure

5E). Additionally, the SVM trained with CD1 male CS and HP data predicted a high pain-like probability for the 4.0 g VFH (0.80), a low pain-like probability for the 0.6 g VFH (0.33), and a boundary pain-like probability for the 1.4 g VFH (0.51) (Figure 5F). Taken together, our analysis suggests that the 4.0 g VFH filament likely evokes a pain-like withdrawal reflex, the 0.6 g VFH likely evokes a non-pain withdrawal reflex, while 1.4 g may be near the mechanical threshold separating pain from non-pain responses.

Proof of Principle 2: High-Speed Imaging Analysis of Paw Withdrawal Reflex Triggered by Peripheral Optogenetic Activation of Different Primary Afferent Populations

Optogenetics is a powerful gain-of-function approach to study primary somatosensory afferents (Arcourt et al., 2017; Barik et al., 2018; Browne et al., 2017; Daou et al., 2013, 2016; Iyer et al., 2014; Murthy et al., 2018). Briefly, channelrhodopsin (ChR2) is expressed in different DRG neuronal populations, and application of transdermal light is used to activate ChR2+ afferents in the skin. Interestingly, optogenetic activation of different populations of DRG neurons reported in the literature so far, all triggered paw withdrawal reflex, raising the question of how to interpret the "sensory experience" evoked by peripheral optogenetics.

Here we tested whether the high-speed imaging and statistical analysis method we established using wild-type mice and natural mechanical stimuli could be applied to the analysis of optically induced withdrawal behaviors of transgenic mice. For this purpose, we generated two mouse lines (Figures 6A and 6B). For the first line (*Trpv1-ChR2* mice), we crossed *Trpv1*^{Cre} (Cavanaugh et al., 2011) to the Ai32 Cre-dependent ChR2 line (Madisen et al., 2012) to express ChR2 in the majority of nociceptors (91% of CRGP+ and 95% of IB4+ nociceptors) and a few large-diameter DRG neurons (13.4% of NFH+ mechanoreceptors [Figure S5], ~80% of DRG neurons in total). For the second line (*Mrgprd-ChR2*), we crossed an inducible Cre mouse line generated in our lab *Mrgprd*^{CreERT2} (Olson et al., 2017), to Ai32 in which ChR2 is specifically expressed in non-peptidergic MRGPRD+ C-nociceptors (Figure S5; ~20%–25% of DRG neurons in total). Because the number of ChR2 expressing neurons is much less in *Mrgprd-ChR2* mice compared with *Trpv1-ChR2* mice, it was necessary to use two copies of *Ai32* alleles (ChR2 homozygous) and high laser power (10 or 20 mW) to activate MRGPRD+ neurons to trigger paw withdrawals (Olson et al., 2017). In contrast, a single copy of *Ai32* allele and low laser power (5 or 10 mW) were sufficient to induce a robust behavior for the *Trpv1-ChR2* line.

Hind paw stimulation with blue laser light (10 mW) of ChR2-only littermate control mice did not cause paw withdrawal, as we have previously reported (Olson et al., 2017; Figure 6C, as indicated by "ctrl"; Video S2), suggesting that the blue laser stimulation itself does not cause non-specific withdrawal behaviors. Blue laser light hind paw stimulation (10 mW) of *Trpv1-ChR2* mice induced paw withdrawal in 100% of mice with a response latency of ~150 ms (Figures 6C and 6D, as indicated by "V1"; Video S3). We then quantified paw height, velocity, and pain score (Figures 6E–6G). Because these transgenic mice are on a mixed C57 and CD1 genetic background and include both males (black dots) and females (pink dots), we calculated PC scores using a combined dataset of C57 and CD1 wild-type male and female mice (Figure 6H; Data S2; see STAR Methods) and predicted the "pain-

like" probability using an SVM trained with CS and HP from male and female CD1 and C57 mice (Figure 6I). Overall, our analysis revealed positive PC scores (Figure 6H) and a high probability of being "pain-like" of *Trpv1-ChR2* mice in response to peripheral optical stimuli (Figure 6I). This is further confirmed when we applied a painkilling cocktail of meloxicam (2 mg/kg) and buprenorphine (0.5 mg/kg) (Tubbs et al., 2011) to these mice, which reversed both PC score and "pain-like" probability (Figures 6H and 6I, as indicated by "V1+PK"). These results suggest that optogenetic activation of TRPV1-ChR2+ afferents triggered "pain-like" sensation at the baseline condition.

Next, we examined behavioral responses induced by blue laser light stimulation of *Mrgprd-ChR2* mice. Similar to *Trpv1-ChR2* mice, we found that 91% of *Mrgprd-ChR2* mice displayed a paw withdrawal with 20 mW of blue laser light stimulation (Figure 6C, as indicated as "M"; Video S2). The blue light-triggered paw response in *Mrgprd-ChR2* mice had a latency of ~700 ms (Figure 6D), which is ~15 times slower than natural mechanical stimuli and 4–5 times slower than blue light-induced responses in *Trpv1-ChR2* mice. Paw height, velocity, and pain score were quantified and PC scores were calculated in a similar manner as *Trpv1-ChR2* mice (Figure 6H; Data S2; see STAR Methods). Interestingly, PC scores of the *Mrgprd-ChR2* mouse paw withdrawal reflex in response to blue laser were, on average, negative (−0.873) (Figure 6H). The SVM also predicted a low probability that these responses were pain-like (Figure 6I). Taken together, these results suggest that acute activation of MRGPRD+ DRG neurons under baseline conditions triggers "non-pain" sensations, despite robust paw withdrawal responses.

To examine whether activation of MRGPRD+ neurons can trigger "pain-like" sensation under other conditions, we induced chronic inflammation in one hind paw of control and *Mrgprd-ChR2* mice by injecting hind paws with complete Freund's adjuvant (CFA) (McCarson, 2015; Figure 6A, as indicated as "M+C" for *"MrgprD-ChR2* & CFA" for experimental paradigm). We found that although blue laser triggered a similarly rate of paw withdrawal responses, pain measurements differed significantly between baseline and CFA conditions (Figures 6E–6G). The PC score (0.578) and SVM predictions both suggest that activation of MRGPRD+ neurons under chronic inflammation evoked a "pain-like" withdrawal reflex (Figures 6H and 6I; Video S2). Subsequent administration of the same analgesic cocktail (indicated as "M+C+PK") inverted PC score (−0.842) and SVM predictions to the non-pain domain, without affecting the response frequency (Figures 6C, 6H, and 6I; Video S2). Our findings indicate that optogenetic activation of non-peptidergic nociceptors induces pain under inflammatory conditions. These results not only highlight the interesting physiology of non-peptidergic nociceptors but demonstrate the power of our method to determine the pain sensation of mice with greatly improved precision.

DISCUSSION

We present here a "mouse pain scale" method that combines high-speed videography and statistical modeling, which increases the reliability and predictive power for using the hind paw withdrawal reflex to assess pain sensation in mice. Compared with the traditional measurements of the hind paw withdrawal (scoring of withdrawal frequency or quantification of withdraw latency), our approach quantifies six distinct behavioral

parameters indicating both the reflexive and affective aspects of nociception on a sub-second scale and combines them into a single index to assess pain sensation in mice on a trial-by-trial basis. With machine learning, we are able to further determine the probability that a given paw withdrawal is "pain-like."

Our work adds to a very short list of studies using high-speed videography in rodents to map the movements following the application of only noxious stimuli to the paw (Blivis et al., 2017; Browne et al., 2017; Mitchell et al., 2014). Compared with the previous work, our study not only identified the presence or absence of "pain" associated sub-second behavior features but developed statistical methods to integrate multiple relevant behavior parameters into a single index that helps quantitatively access the mouse pain state. Moreover, the prior studies did not examine responses to innocuous stimuli. Given the overlapping behavioral parameters triggered by noxious and innocuous stimuli, it is challenging to identify the threshold that distinguishes "pain" and "non-pain" behaviors. By comparing and analyzing behaviors induced by both noxious and innocuous stimuli and combining parameters through statistical modeling, we established the threshold that differentiates behavioral kinematics indicating "pain-like" from those indicating "non-pain" sensory experiences.

As a proof-of-principle example, our results with VFHs showed that that the 4.0 g VFH induced a "pain-like" paw withdrawal, whereas 0.6 and 1.4 g induced withdrawal behaviors more similar to those induced by CS and DB. Interestingly, mice showed similar pain associated affective features (i.e., pain score) in response to all three VFHs (Figure 5D). Thus, without using high-speed imaging and composite PCA, which includes both reflexive and affective aspects of nociception, it would be very difficult to distinguish the "quality" of these responses. Our result is very interesting in light of recent genetic studies ablating the mechanosensitive ion channel PIEZO2, which is critical for touch sensation (Coste et al., 2010; Ranade et al., 2014; Woo et al., 2014). These studies place the mechanical threshold that separates "pain" from "non-pain" at approximately 1.5–3.0 g, which is similar to what is indicated by our method (1.4 g is around the "mechanical threshold").

The other proof-of-principle experiments was optogenetic activation of TRPV1-ChR2+ (~80% DRG neurons are ChR2+) and MRGPRD-ChR2+ (~20% DRG neurons are ChR2+) non-peptidergic afferent fibers. Non-peptidergic MRGPRD+ nociceptors are a molecularly and anatomically unique class of small-diameter primary somatosensory neurons (Zylka et al., 2005). They are polymodal high-threshold C fibers responsive to mechanical, chemical, and thermal stimuli on the basis of physiological recordings (Dussor et al., 2008; Liu et al., 2012; Rau et al., 2009). In addition, genetic ablation studies suggest that these primary afferents are tuned for detecting noxious mechanical stimuli (Cavanaugh et al., 2009). Paradoxically, however, when non-peptidergic nociceptors were acutely activated by either chemogenetics or optogenetics using place preference assays, no place aversion was observed (Beaudry et al., 2017; Vrontou et al., 2013). These gain-of-function studies raise the question of whether acute activation of these neurons *in vivo* is sufficient to trigger pain sensation. Here we analyzed paw withdrawal reflex upon acute peripheral optogenetic activation of MRGPRD-ChR2+ neurons using our approach. Although acute activation of this neuronal population leads to almost 100% of paw withdrawal at baseline conditions, our PCA and SVM analyses indicate that these withdrawals fall into "non-painful" domain

(Figure 6). This is in great contrast to the light-evoked "pain-like" paw withdrawal reflex of *Trpv1-ChR2* mice. Our result supports previous operant assays, suggesting that under baseline conditions, acute activation of MRGPRD+ non-peptidergic nociceptors is not sufficient to evoke "pain" sensation. This is also consistent with human self-report of "tingling" but not "pain" sensation after taking beta-alanine, a chemical that activates MRGPRD (Bodybuilding.com, 2013). Interestingly, the VFH mechanical forces used in the previous loss-of-function study were 1.2 g and below (Cavanaugh et al., 2009). Because our data indicate that 1.4 g is close to the mouse mechanical pain threshold at baseline conditions, results using 1.2 g may indicate a change in the sense of touch but not necessarily mechanical pain. Collectively, these studies (both loss-of-function and gain-of-function) suggest that non-peptidergic neurons may normally play a role in mechanical but not "pain" sensation.

In addition, we noticed that for both *Trpv1-ChR2* and CFA-injected *Mrgprd-ChR2* mice, the high "pain-like" probabilities of light-evoked behaviors were driven mainly by the pain score (i.e., orbital tightening, paw shaking, jumping, and paw guarding) but not paw height or velocity (Figure 6). This is in contrast to the 4.0 g VFH, in which the high probabilities of being "pain-like" are driven by the contribution of paw height and velocity (Figure 6). Though the neuronal mechanisms underlying these differences is not fully understood yet, our results reveal the complexity of "pain expression phenotypes" in animals and highlight the strength of including parameters indicating both reflexive (paw height and velocity) and affective (pain score) aspects of pain for analysis (Corder et al., 2017). As more labs use peripheral optogenetic approaches to study the somatosensory system and neural circuits underlying pain sensation, our results also suggest caution against presumptions for interpreting light-induced behaviors that are based mainly on the neuronal population that expresses ChR2.

STAR★METHODS

LEAD CONTACT AND MATERIALS AVAILABILITY

Further information and requests for resources and reagents should be directed to and will be fulfilled by the Lead Contact, Dr. Wenqin Luo (luow@pennmedicine.upenn.edu). For the distribution of materials and data, we have uploaded all raw data and code to Mendeley (https://doi.org/10.17632/mcygb8762v.1) (URL: https://data.mendeley.com/datasets/mcygb8762v/1) and Github (URL: https://github.com/longdecision/PainAssaySVM). The purpose of this code is for researchers to use their own datasets, or the data presented in this paper, for SVM machine learning to make predictions about the sensation evoked from different somatosensory stimuli applied to the mouse hind paw.

EXPERIMENTAL MODEL AND SUBJECT DETAILS

Mouse strains—Mice for behavior testing were maintained in a conventional animal facility in the John Morgan building at the University of Pennsylvania. Mice for *in vivo* calcium imaging were maintained in a barrier animal facility at the Johns Hopkins School of Medicine. All procedures were conducted according to animal protocols approved by the university Institutional Animal Care and Use Committee (IACUC) and in accordance with

National Institutes of Health (NIH) guidelines. CD1 male and female mice were purchased from Charles River Laboratories and C57BL/6J male and female mice were purchased from Jackson Laboratories. MRGPRD-ChR2 mice, $Mrgprd^{CreERT2};ChR2^{f/f}$ (Ai32 homozygous), were generated in our lab as previously described (Olson et al., 2017). *Mrgprd-ChR2* mice were treated with tamoxifen between P10-P17 to induce robust ChR2 expression in MRGPRD^{+} neurons. *Trpv1-ChR2* mice (*Trpv1^{Cre}*;*ChR2^{f/+}* (Ai32 heterozygous)), were generated by crossing *Trpv1^{Cre}* and Ai32 together. Pirt-GCAMP6 mice were generated by crossing *Pirt^{Cre}* mice to *Rosa-GCAMP6* mice, as previously described (Kim et al., 2016). *Trpv1^{Cre}* (stock no. 017769) (Cavanaugh et al., 2011) and *Rosa-ChR2-eYFP* (Ai32) (stock no. 012569) (Madisen et al., 2012) mice were purchased from the Jackson Laboratories. For all behavioral studies adult mice, of each sex, were used that were at least 8 weeks old. The sex of animals tested is clearly indicated in the text and in the figures. All mice were group housed with 5 animals per cage.

METHOD DETAILS

Whole animal L4 DRG neuron calcium imaging combined with hind paw stimulation—The L4 DRG of Pirt-GCAMP6 mice was surgically exposed and imaged, with subsequent data analysis performed using ImageJ (NIH) as previously described (Kim et al., 2016). Briefly, for all imaging experiments, mice at 2 months or older were anesthetized by i.p. injection of chloral hydrate (560 mg/kg). After deep anesthesia was reached, the animal's back was shaved and aseptically prepared. Ophthalmic ointment (Lacrilube; Allergen Pharmaceuticals) was applied to the eyes to prevent drying. During the surgery, mice were kept on a heating pad (DC temperature controller, FHC) to maintain body temperature at $37 \pm 0.5°C$ as monitored by a rectal probe. Dorsal laminectomy in DRG was performed usually at spinal level L6 to S1 below the lumbar enlargement (occasionally at lower than S1) but without removing the dura. A 2-cm-long midline incision was made around the lower part of the lumbar enlargement area; next, the paravertebral muscles were dissected away to expose the lower lumbar part which surrounds (L3–L5) vertebra bones. The L4 DRG transverse processes were exposed and cleaned. Using small rongeurs, we removed the surface aspect of the L4 DRG transverse process near the vertebra to expose the underlying DRG without damaging the DRG and spinal cord. Bleeding from the bone was stopped using styptic cotton. After surgery, mice were laid down in the abdomen-down position on a custom-designed microscope stage. The spinal column was stabilized using custom-designed clamps to minimize movements caused by breathing and heart beats. *In vivo* imaging of whole L4 DRG in live mice could be performed for 1–6 hr immediately after the surgery.

The four stimuli (cotton swab, dynamic brush, light pinprick, and heavy pinprick) were applied to the freely hanging hind paw as described in the following section. The microscope stage was fixed under a laser-scanning confocal microscope (Leica LSI microscope system), which was equipped with macrobased, large-objective, and fast EM-CCD camera. Live images were acquired at typically eight to ten frames with 600 Hz in frame-scan mode per 6–7 s, at depths below the dura ranging from 0 to 70 mm, using a 5X 0.5 NA macro dry objective at typically 512 X 512 pixel resolution with solid diode lasers (Leica) tuned at 488 and at 532 nm wavelength and emission at 500–550 nm for green

fluorescence. DRG neurons were at the focal plane, and imaging was monitored during the activation of DRG neuron cell bodies by peripheral stimuli. The imaging parameters were chosen to allow repeated imaging of the same cell over many stimuli without causing damage to the imaged cells or to surrounding tissue. Raw image stacks (512X512 to 1024 X 1024 pixels in the x–y plane and 20–30 mm voxel depth; typically 10 optical sections) were imported into ImageJ (NIH) for analysis. A neuron displaying Ca^{2+} F/F0 higher than 20% is considered as a positively responsive neuron.

High-Speed Videography—To capture mouse kinematic movement features at high temporal resolution, we recorded behaviors at 500 or 1000 frames per second (fps) with a high-speed camera (FastCAM UX100 800K-M-4GB - Monochrome 800K with 4GB memory) and attached lens (NikonZoom Wide Angle Telephoto 24–85mm f2.8). With a tripod with geared head for Photron UX100, the camera was placed at a ~45° angle at ~1-2 feet away from the Plexiglas holding chambers where mice performed behaviors. The camera was maximally activated with far-red shifted 10 mW LED light that mice cannot detect and thus would not disturb their behaviors. All data were collected and annotated on a Dell laptop computer with FastCAM NI DAQ software that is designed to synchronize Photron slow motion cameras with the M series integrated BNC Data Acquisition (DAQ) units from National Instruments.

Somatosensory behavior assays—Mice were acclimated to a small rectangular or round Plexiglas chamber where they could move freely but could not stand up. Selected mechanical stimuli were delivered to one hind paw when mice were calm, still, and with all four paws on the raised mesh platform. Mice were habituated to the testing chambers for one week before behavioral tests were performed. C57 and CD1 mouse lines were used, with an equal number (10) of male and female mice included. Some animals were tested multiple times, and in these cases, the quantification of behavior features was averaged across multiple trials for a given animal. Stimuli were applied to the hind paw of each mouse through the mesh floor. Cotton swab tests consisted of gentle contact between the cotton Q-tip and the hind paw of the mouse. Dynamic brush tests were performed by wiping a concealer makeup brush (e.l.f.™, purchased at the CVS) across the hind paw from back to front. Light pinprick tests were performed by gently touching a pin (Austerlitz Insect Pins®) to the hind paw of the mouse. The pin was withdrawn as soon as contact was observed. Heavy pinprick tests were performed by sharply pressing this pin into the paw so that it was pushed upward with force. The pin was withdrawn as soon as approximately 1/3 of the pins length had passed through the mesh. For application of von Frey hairs (VFHs, Stoelting Company, 58011), we used 3 different forces: 0.6 g, 1.4 g, and 4 g. As previously described, each VFH was directed at the center of the plantar paw and pressed upward until the filament bent (Cui et al., 2016). For the four natural stimuli and VFHs, an animal that did not respond within 2 s of stimulus delivery was considered as non-responsive. For inducing chronic inflammatory pain, ~10 μL of Complete Freud's Adjuvant, CFA (Sigma, F5881) was injected into the plantar surface of 3% isoflurane anesthetized mice as previously published (Liu et al., 2010). For analgesic painkiller treatment, a 50 μL cocktail of meloxicam (2 mg/kg, Penn Veterinary Hospital) and buprenorphine (0.5 mg/kg, Henry

Schein Animal Health, 059122) were injected subcutaneously into the back of restrained mice. Approximately 45 minutes separated injection of painkillers and behavioral testing.

Scoring behavioral movement features—Onset of head turn is defined as a movement of the animal's head from a stationary position toward the stimulated hind paw. Paw height and paw velocity were extracted from the high speed videos and processed with Photron FastCAM software. Paw height was scored in millimeters as the distance from the mesh floor to the highest point following paw stimulation. Paw velocity was scored as the distance in millimeters from initial paw lift to the highest point, divided by the time in seconds between the two points. The pain score is a composite score of four individual behavior features: orbital tightening, paw shake, paw guard, and jumping. For example, if a given animal displayed 1/4 of those features it would receive a pain score of 1. An animal was scored as displaying an orbital tightening if its eyes went from fully open to partially or fully closed following stimulus application. Paw shaking was defined as high frequency paw flinching. Jumping was defined as all four paws off the mesh floor at the same time following a stimulus application. Lastly, paw guard was defined as any abnormal placement of the paw back to the mesh floor following stimulus application. We were not blind to the strain when scoring behaviors of wild-type mice as CD1 mice are white while C57 mice are black. However, we are blind to the stimulus type and VFH forces.

Peripheral optogenetics—To optically activate the nerve terminals of *Trpv1-ChR2* and *Mrgprd-ChR2* mice through the hind paw skin of freely behaving animals, mice were placed in the same setup and given the one-week habituation as described above for natural stimuli. For optogenetic experiments, the operator was always blinded to genotype during the testing and scoring. Only when experiments were completed, we matched the mouse's ear tag number with its genotype to plot the data in graphical form. In terms of analgesic treatment, one operator randomly injected mice, while a different operator performed the experiments blinded to which mice received analgesia. Lastly, the experimenter scoring the data was blinded to which groups received analgesia during testing. To induce a behavioral response in *Mrgprd-ChR2* mice, we shined 20 mW 473 nm blue laser light (Shanghai Laser and Optics Century, BL473T8–150FC/ADR-800A) to one of the hind paws. To induce a behavioral response in *Trpv1-ChR2* mice, 10 mW 473 nm blue laser light was used. We pulsed the light in all experiments at 10 hz sine wave which was generated by a pulse generator (Agilent 10MHZ Function Waveform Generator, 33210A) connected to the laser source. For all stimulations, the laser light was delivered via an FC/PC optogenetic patch cable with a 200 mm core opening (ThorLabs, M72L01) and there was approximately 1 cm of space between the cable terminal and the hind paw skin. Light power intensity for each experiment was measured with a digital power meter with a 9.5 mm aperture (ThorLabs, PM100A). Lastly, light was only applied to mice standing on all four paws, calm and still, but not in the process of grooming or other actions.

Tissue preparation and histology—Procedures were conducted as previously described (Fleming et al., 2012). Briefly, mice used for immunostaining were transcardially perfused with 4% PFA/PBS, and dissected tissue (either skin or spinal cord and DRGs/TGs) was post-fixed for 2 hr in 4% PFA/PBS at 4°C. Tissue used for immunostaining was cryo-

protected in 30% sucrose/PBS (4% overnight) before freezing, except the c-FOS experiments where tissue was kept at room temperature and proceeded directly for vibratome sectioning. Frozen glabrous skin, DRG/spinal cord, and TG sections (20–30 mm) were cut on a Leica CM1950 cryostat. Immunostaining of sectioned TG, DRG, spinal cord, and glabrous skin tissue, was performed as described previously (Fleming et al., 2012; Niu et al., 2013). The following antibodies were used: chicken anti-GFP, 1:1000 (Aves, GFP-1020), rabbit anti-CGRP, 1:1000 (Immunostar, 24112), conjugated IB4-Alex594, 1:200 (Molecular Probes, I21411), guinea pig anti-VGLUT1, 1:1000 (Fisher, AB5905), rabbit anti-NFH, 1:1000 (Sigma, N4142), and rabbit anti-cFOS, 1:100, (Santa Cruz, sc-52).

c-FOS staining—For c-FOS staining following optogenetic stimulation, *Mrgprd-ChR2* mice were manually restrained and scuffed for 10 minutes while 10 Hz 20 mW blue light was shined directly to the ear and ear canal. We waited approximately 1.5 hours after optogenetic stimulation, and transcardially perfused the mouse with 4% PFA followed by a four hour post-fixation period. We then cut 50 mm sections with a vibratome followed by performing free-floating immunohistochemistry (Fleming et al., 2012).

QUANTIFICATION AND STATISTICAL ANALYSIS

An exploratory factor analysis with orthogonal Varimax rotation was conducted with SPSS to determine which of the initial eleven parameters contributed to at least 10% of the variance. We initially found that four parameters (total paw time, paw airtime, paw at apex, and paw time after apex) were highly correlated so we only used one (paw air-time) for subsequent analysis, leaving a total of eight parameters (Figure S3A). We then performed three iterations of an exploratory factor analysis using an eigenvalue cut-off of 1.0 with each being confirmed to have patterned relationships with the bartlett's test of sphericity (p < 0.001). We then removed parameters that had either low factor loadings or cross-loaded onto multiple factors (Figure S3B). We considered factor loading coefficients of < 0.35 as low and not significantly contributing to a particular principle component. The first iteration revealed three Principle Components (in blue) that accounted for 62.7% of variance (Figure S3B – Iteration 1). Analysis of the rotated component matrix revealed that response time and head duration cross loaded onto multiple principle components so they were removed. The second iteration revealed two Principle Components (in blue) that accounted for 60.9% of variance (Figure S3B – Iteration 2). Analysis of the rotated component matrix revealed that full turn duration cross loaded onto multiple principle components and total time had a low factor loading (i.e., <0.35) so they were removed. The final iteration revealed a single Principle Component (in blue) that accounted for 57.3% of variance with paw-air time having a low factor loading (Figure S3B – Iteration 3). We settled on three of the remaining parameters (paw height, paw velocity, and pain score).

We performed dimension-reduction with a Principle Component Analysis using the paw height, paw-air time, paw velocity, and pain score. The contributing weights, as represented by eigenvalue, for each syllable of each genotype and sex database, were determined using SAS. We could then combine normalized z-scores for each syllable into a single one-dimensional principle component for every stimulus trial. This process was conducted independently for males and females of both genotypes, generating their own set of

eigenvalues for each syllable that could then be used to transform the three-dimensional data (paw height, paw velocity, and pain score) to a single dimension (Table 1). Individual behavioral movement features, VFH filaments, and TRPV1-ChR2 and MRGPRD-ChR2 groups were compared using ANOVA followed by Tukey's multiple comparison with p value threshold set to 0.05. All results of statistical analyses can be found within the text, figures, and figure legends.

Machine learning—We classified paw withdrawal reflexes into "pain" and "non-pain" categories, using four measurements obtained from the highspeed imaging data: paw-air time, paw velocity, paw height and pain score. A classification pipeline consisted of the following steps (scikit-learn, 0.18.1): 1) the first principal component (PCA1) was derived from the training data, 2) the first component scores for the training data were used to train a support vector machine (SVM) with radial basis function kernels (kernel coefficient gamma = 1, penalty parameter C = 1), and 3) for a given trial, the SVM predicts the probability of the presence of a "pain" response based on that trial's component score for the training-data PCA1. The data used to generate the PCA1 and train the SVM for each figure can be seen in Table 1.

Supplementary Material

Refer to Web version on PubMed Central for supplementary material.

ACKNOWLEDGMENTS

REFERENCES

Akintola T, Raver C, Studlack P, Uddin O, Masri R, and Keller A (2017). The grimace scale reliably assesses chronic pain in a rodent model of trigeminal neuropathic pain. Neurobiol Pain 2, 13–17. [PubMed: 29450305]

Arcourt A, Gorham L, Dhandapani R, Prato V, Taberner FJ, Wende H, Gangadharan V, Birchmeier C, Heppenstall PA, and Lechner SG (2017). Touch receptor-derived sensory information alleviates acute pain signaling and fine-tunes nociceptive reflex coordination. Neuron 93, 179–193. [PubMed: 27989460]

Barik A, Thompson JH, Seltzer M, Ghitani N, and Chesler AT (2018). A brainstem-spinal circuit controlling nocifensive behavior. Neuron 100, 1491–1503.e3. [PubMed: 30449655]

Barrot M (2012). Tests and models of nociception and pain in rodents. Neuro-science 211, 39–50.

Beaudry H, Daou I, Ase AR, Ribeiro-da-Silva A, and Sdguela P (2017). Distinct behavioral responses evoked by selective optogenetic stimulation of the major TRPV1+ and MrgD+ subsets of C-fbers. Pain 158, 2329–2339. [PubMed: 28708765]

Blivis D, Haspel G, Mannes PZ, O'Donovan MJ, and Iadarola MJ (2017). Identification of a novel spinal nociceptive-motor gate control for Ad pain stimuli in rats. eLife 6, e23584. [PubMed: 28537555]

Bodybuilding.com (2013). Beta alanine - itchy?.https://forum.bodybuilding.com/showthread.php?t=152836051&page=1.

Bove G (2006). Mechanical sensory threshold testing using nylon monofilaments: the pain field's "tin standard.". Pain 124, 13–17. [PubMed: 16846693]

Bradman MJ, Ferrini F, Salio C, and Merighi A (2015). Practical mechanical threshold estimation in rodents using von Frey hairs/Semmes-Weinstein monofilaments: towards a rational method. J. Neurosci. Methods 255, 92–103. [PubMed: 26296284]

Browne LE, Latremoliere A, Lehnert BP, Grantham A, Ward C, Alexandre C, Costigan M, Michoud F, Roberson DP, Ginty DD, and Woolf CJ (2017). Time-resolved fast mammalian behavior reveals the complexity of protective pain responses. Cell Rep. 20, 89–98. [PubMed: 28683326]

Cavanaugh DJ, Lee H, Lo L, Shields SD, Zylka MJ, Basbaum AI, and Anderson DJ (2009). Distinct subsets of unmyelinated primary sensory fibers mediate behavioral responses to noxious thermal and mechanical stimuli. Proc. Natl. Acad. Sci. USA 706, 9075–9080.

Cavanaugh DJ, Chesler AT, Jackson AC, Sigal YM, Yamanaka H, Grant R, O'Donnell D, Nicoll RA, Shah NM, Julius D, and Basbaum AI (2011). Trpvl reporter mice reveal highly restricted brain distribution and functional expression in arteriolar smooth muscle cells. J. Neurosci 37, 5067–5077.

Cheng L, Duan B, Huang T, Zhang Y, Chen Y, Britz O, Garcia-Campmany L, Ren X, Vong L, Lowell BB, et al. (2017). Identification of spinal circuits involved in touch-evoked dynamic mechanical pain. Nat. Neurosci 20, 804–814. [PubMed: 28436981]

Corder G, Tawfik VL, Wang D, Sypek EI, Low SA, Dickinson JR, Sotoudeh C, Clark JD, Barres BA, Bohlen CJ, and Scherrer G (2017). Loss of μ opioid receptor signaling in nociceptors, but not microglia, abrogates morphine tolerance without disrupting analgesia. Nat. Med 23, 164–173. [PubMed: 28092666]

Coste B, Mathur J, Schmidt M, Earley TJ, Ranade S, Petrus MJ, Dubin AE, and Patapoutian A (2010). Piezo1 and Piezo2 are essential components of distinct mechanically activated cation channels. Science 330, 55–60. [PubMed: 20813920]

Cui L, Miao X, Liang L, Abdus-Saboor I, Olson W, Fleming MS, Ma M, Tao YX, and Luo W (2016). Identification of early RET+ deep dorsal spinal cord interneurons in gating pain. Neuron 97, 1137–1153.

Daou I, Tuttle AH, Longo G, Wieskopf JS, Bonin RP, Ase AR, Wood JN, De Koninck Y, Ribeiro-da-Silva A, Mogil JS, and Seguela P (2013). Remote optogenetic activation and sensitization of pain pathways in freely moving mice. J. Neurosci 33, 18631–18640. [PubMed: 24259584]

Daou I, Beaudry H, Ase AR, Wieskopf JS, Ribeiro-da-Silva A, Mogil JS, and Seguela P (2016). Optogenetic silencing of Nav1.8-positive afferents alleviates inflammatory and neuropathic pain. eNeuro 3, ENEURO.0140-15.2016.

Deuis JR, Dvorakova LS, and Vetter I (2017). Methods used to evaluate pain behaviors in rodents. Front. Mol. Neurosci 70, 284.

Duan B, Cheng L, Bourane S, Britz O, Padilla C, Garcia-Campmany L, Krashes M, Knowlton W, Velasquez T, Ren X, et al. (2014). Identification of spinal circuits transmitting and gating mechanical pain. Cell 759, 1417–1432.

Dussor G, Zylka MJ, Anderson DJ, and McCleskey EW (2008). Cutaneous sensory neurons expressing the Mrgprd receptor sense extracellular ATP and are putative nociceptors. J. Neurophysiol 99, 1581–1589. [PubMed: 18234974]

Fleming MS, Ramos D, Han SB, Zhao J, Son Y-JJ, and Luo W (2012). The majority of dorsal spinal cord gastrin releasing peptide is synthesized locally whereas neuromedin B is highly expressed in pain- and itch-sensing somatosensory neurons. Mol. Pain 8, 52. [PubMed: 22776446]

Hung CH, Wang JC, and Strichartz GR (2015). Spontaneous chronic pain after experimental thoracotomy revealed by conditioned place preference: morphine differentiates tactile evoked pain from spontaneous pain. J. Pain 76, 903–912.

Iyer SM, Montgomery KL, Towne C, Lee SY, Ramakrishnan C, Deisseroth K, and Delp SL (2014). Virally mediated optogenetic excitation and inhibition of pain in freely moving nontransgenic mice. Nat. Biotechnol 32, 274–278. [PubMed: 24531797]

Kim YS, Anderson M, Park K, Zheng Q, Agarwal A, Gong C, Saijilafu, Young L, He S, LaVinka PC, et al. (2016). Coupled activation of primary sensory neurons contributes to chronic pain. Neuron 97, 1085–1096.

Kim AJ, Fenk LM, Lyu C, and Maimon G (2017). Quantitative predictions orchestrate visual signaling in Drosophila. Cell 768, 280–294.e12.

Lambert GA, Mallos G, and Zagami AS (2009). Von Frey's hairs—a review of their technology and use-a novel automated von Frey device for improved testing for hyperalgesia. J. Neurosci. Methods 777, 420–426.

Langford DJ, Bailey AL, Chanda ML, Clarke SE, Drummond TE, Echols S, Glick S, Ingrao J, Klassen-Ross T, Lacroix-Fralish ML, et al. (2010). Coding of facial expressions of pain in the laboratory mouse. Nat. Methods 7, 447–449. [PubMed: 20453868]

Le Bars D, Gozariu M, and Cadden SW (2001). Animal models of nociception. Pharmacol. Rev. 53, 597–652. [PubMed: 11734620]

Liu Y, Abdel Samad O, Zhang L, Duan B, Tong Q, Lopes C, Ji R-RR, Lowell BB, and Ma Q (2010). VGLUT2-dependent glutamate release from nociceptors is required to sense pain and suppress itch. Neuron 68, 543–556. [PubMed: 21040853]

Liu Q, Sikand P, Ma C, Tang Z, Han L, Li Z, Sun S, LaMotte RH, and Dong X (2012). Mechanisms of itch evoked by p-alanine. J. Neurosci 32, 14532–14537. [PubMed: 23077038]

Madisen L, Mao T, Koch H, Zhuo J-M, Berenyi A, Fujisawa S, Hsu Y-WAW, Garcia AJ 3rd, Gu X, Zanella S, et al. (2012). A toolbox of Cre-dependent optogenetic transgenic mice for light-induced activation and silencing. Nat. Neurosci. 75, 793–802.

Mauderli AP, Acosta-Rua A, and Vierck CJ (2000). An operant assay of thermal pain in conscious, unrestrained rats. J. Neurosci. Methods 97, 19–29. [PubMed: 10771071]

McCarson KE (2015). Models of inflammation: carrageenan- or complete Freund's adjuvant (CFA)-induced edema and hypersensitivity in the rat. Curr. Protoc. Pharmacol Chapter 5, Unit 5.4.

Mitchell K, Lebovitz EE, Keller JM, Mannes AJ, Nemenov MI, and Ia-darola MJ (2014). Nociception and inflammatory hyperalgesia evaluated in rodents using infrared laser stimulation after Trpv1 gene knockout or resiniferatoxin lesion. Pain 755, 733–745.

Mogil JS (2009). Animal models of pain: progress and challenges. Nat. Rev. Neurosci. 70, 283–294.

Muijres FT, Elzinga MJ, Melis JM, and Dickinson MH (2014). Flies evade looming targets by executing rapid visually directed banked turns. Science 344, 172–177. [PubMed: 24723606]

Murthy SE, Loud MC, Daou I, Marshall KL, Schwaller F, Kuhnemund J, Francisco AG, Keenan WT, Dubin AE, Lewin GR, and Patapoutian A (2018). The mechanosensitive ion channel Piezo2 mediates sensitivity to mechanical pain in mice. Sci. Transl. Med 70, eaat9897.

Nag S, and Mokha SS (2016). Activation of the trigeminal α2-adrenoceptor produces sex-specific, estrogen dependent thermal antinociception and antihyperalgesia using an operant pain assay in the rat. Behav. Brain Res 374, 152–158.

Niu J, Ding L, Li JJ, Kim H, Liu J, Li H, Moberly A, Badea TC, Duncan ID, Son YJ, et al. (2013). Modality-based organization of ascending somatosensory axons in the direct dorsal column pathway. J. Neurosci. 33, 17691–17709. [PubMed: 24198362]

Olson W, Abdus-Saboor I, Cui L, Burdge J, Raabe T, Ma M, and Luo W (2017). Sparse genetic tracing reveals regionally specific functional organization of mammalian nociceptors. eLife 6, e29507. [PubMed: 29022879]

Ranade SS, Woo SH, Dubin AE, Moshourab RA, Wetzel C, Petrus M, Mathur J, Begay V, Coste B, Mainquist J, et al. (2014). Piezo2 is the major transducer of mechanical forces for touch sensation in mice. Nature 576, 121–125.

Rau KK, McIlwrath SL, Wang H, Lawson JJ, Jankowski MP, Zylka MJ, Anderson DJ, and Koerber HR (2009). Mrgprd enhances excitability in specific populations of cutaneous murine polymodal nociceptors. J. Neurosci 29, 8612–8619. [PubMed: 19571152]

Rohrs EL, Kloefkorn HE, Lakes EH, Jacobs BY, Neubert JK, Caudle RM, and Allen KD (2015). A novel operant-based behavioral assay of mechanical allodynia in the orofacial region of rats. J. Neurosci. Methods 248, 1–6. [PubMed: 25823368]

Tubbs JT, Kissling GE, Travlos GS, Goulding DR, Clark JA, King-Herbert AP, and Blankenship-Paris TL (2011). Effects of buprenorphine, meloxicam, and flunixin meglumine as postoperative analgesia in mice. J. Am. Assoc. Lab. Anim. Sci 50, 185–191. [PubMed: 21439211]

Tuttle AH, Molinaro MJ, Jethwa JF, Sotocinal SG, Prieto JC, Styner MA, Mogil JS, and Zylka MJ (2018). A deep neural network to assess spontaneous pain from mouse facial expressions. Mol. Pain 14, 1744806918763658. [PubMed: 29546805]

Vrontou S, Wong AM, Rau KK, Koerber HR, and Anderson DJ (2013). Genetic identification of C fibres that detect massage-like stroking of hairy skin in vivo. Nature 493, 669–673. [PubMed: 23364746]

Wolman MA, Jain RA, Liss L, and Granato M (2011). Chemical modulation of memory formation in larval zebrafish. Proc. Natl. Acad. Sci. USA 108, 15468–15473. [PubMed: 21876167]

Woo SH, Ranade S, Weyer AD, Dubin AE, Baba Y, Qiu Z, Petrus M, Miyamoto T, Reddy K, Lumpkin EA, et al. (2014). Piezo2 is required for Merkel-cell mechanotransduction. Nature 509, 622–626. [PubMed: 24717433]

Yuan T, Li J, Shen L, Zhang W, Wang T, Xu Y, Zhu J, Huang Y, and Ma C (2016). Assessment of itch and pain in animal models and human subjects. Adv. Exp. Med. Biol 904, 1–22. [PubMed: 26900059]

Zylka MJ, Rice FL, and Anderson DJ (2005). Topographically distinct epidermal nociceptive circuits revealed by axonal tracers targeted to Mrgprd. Neuron 45, 17–25. [PubMed: 15629699]

Highlights

- High-speed videography identifies sub-second pain-related behavioral features

- Statistical modeling converts behavioral features to a single index (mouse pain scale)

- Mouse pain scale classifies sensation induced by Von Frey hair stimulation

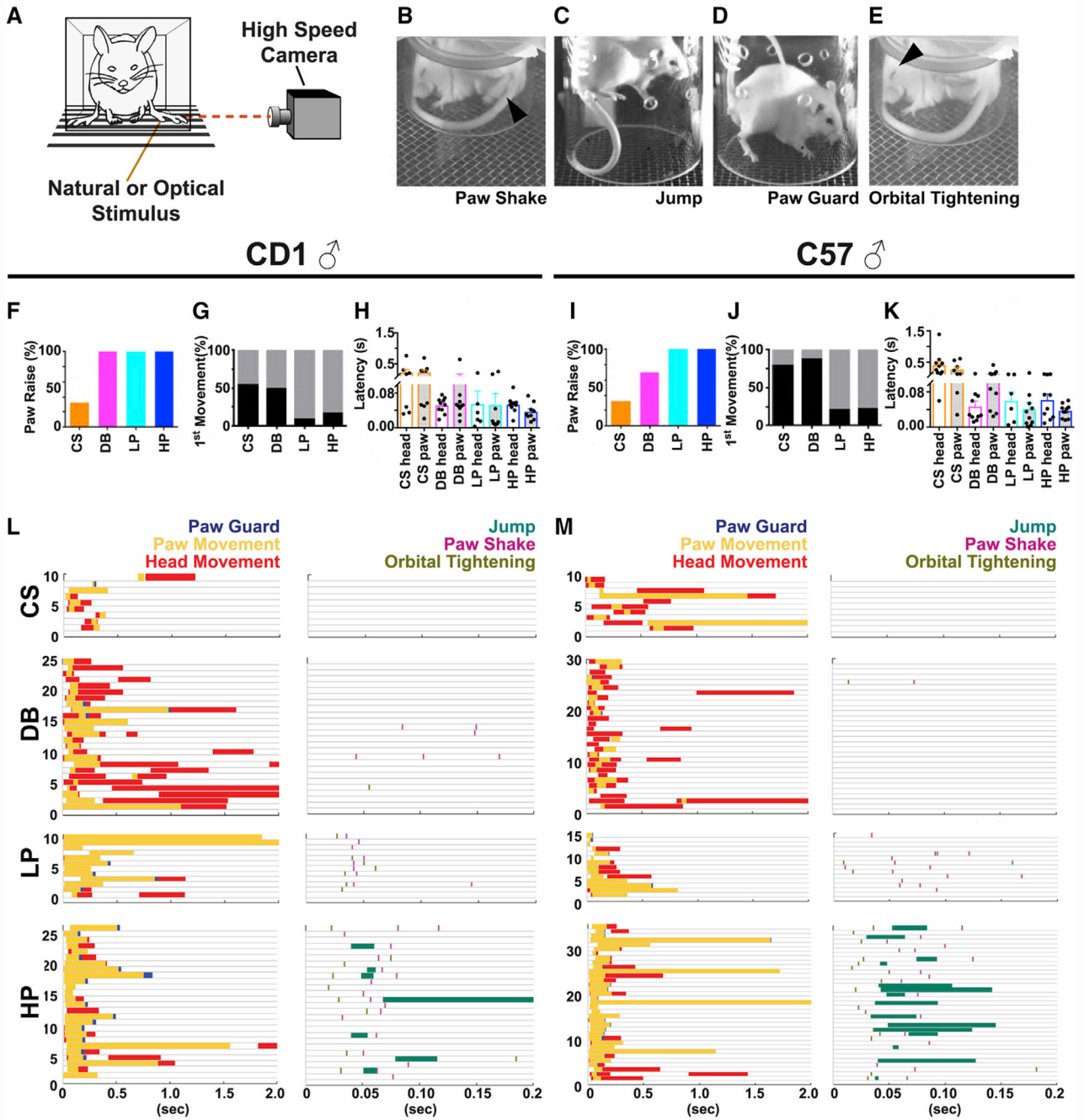- Mouse pain scale classifies sensation triggered by optogenetic activation

Figure 1. Sub-second Temporal Mapping of Mouse Behavioral Features in Response to Natural Mechanical Stimuli

(A) Schematic of behavioral setup showing lateral placement of high-speed camera in relation to contained yet freely behaving mouse.

(B–E) Representative single-frame images taken from high-speed videos of CD1 male mice following stimulation. Black arrows indicate paw shake in (B) and orbital tightening in (E), while animal jumping with paws off the mesh is shown in (C) and paw guarding with abnormal paw placement back on mesh floor is shown in (D). (F–K) Percentage of paw raises (F), first movement being either head (black) or paw (gray) (G), and latency of head

and paw movement for each stimulus in (H) CD1 and percentage of paw raises (I), first movement a head (black) or paw (gray) (J), and latency of head and paw movement for each stimulus (K) in C57 male mice. (L and M) Raster plot of CD1 (L) and C57 (M) mice sub-second behaviors (color-coded) in response to cotton swab (CS), dynamic brush (DB), light pinprick (LP), and heavy pinprick (HP) during either the first 2 s or the first 200 ms. For each raster plot, time of behavior shown on x axis, while each trial per animal is on y axis. n = 10 animals for all groups in (F)–(M).
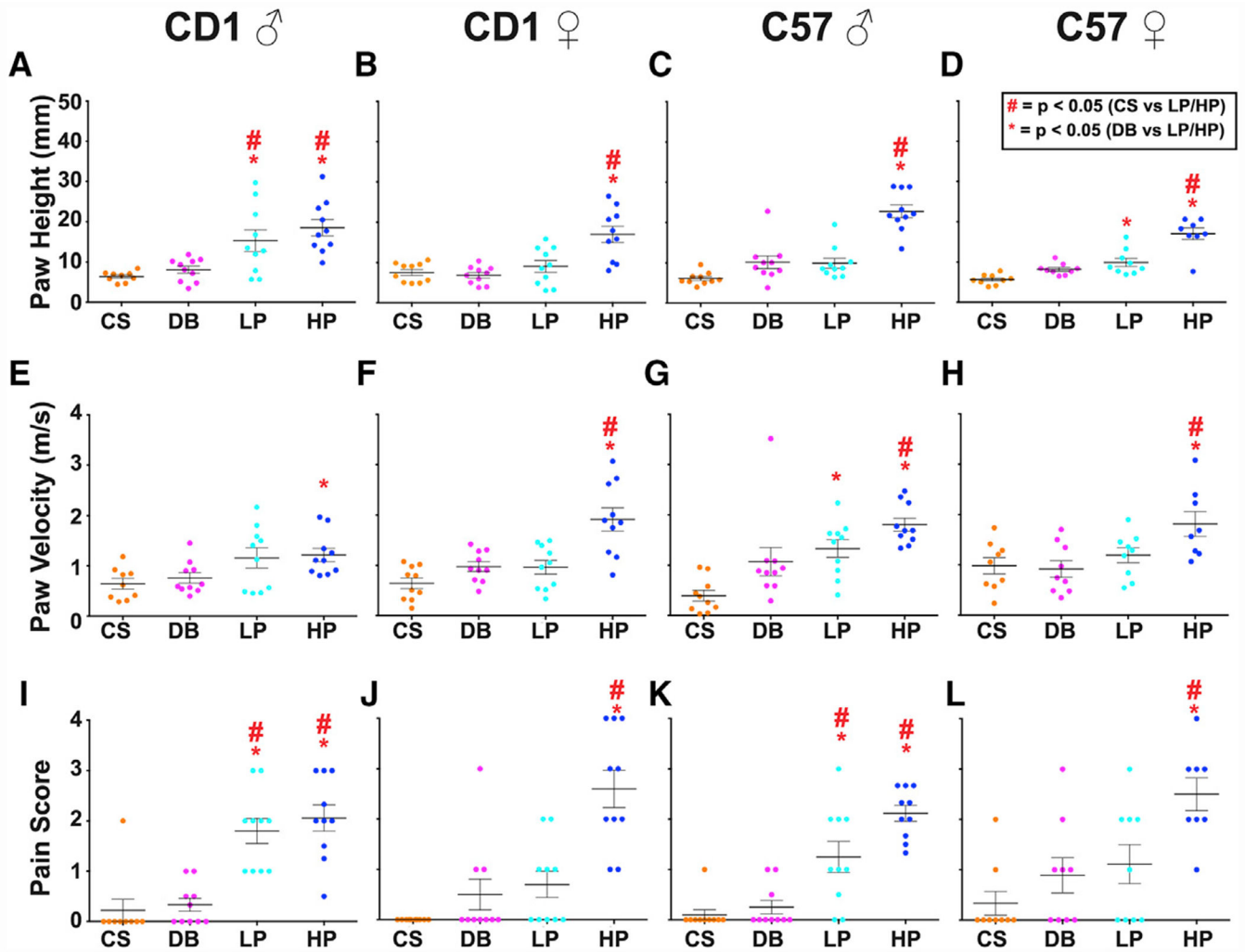
Figure 2. Quantification of the Three Behavior Parameters Showing Statistical Differences between Innocuous and Noxious Stimuli

Each dot represents a given trial. Statistical significance between stimuli is determined using one-way ANOVA followed by Tukey's multiple comparison test. Red stars represent p values < 0.05 when comparing CS with LP or CS with HP (LP or HP > CS), while red asterisks represent p values < 0.05 when comparing DB with LP or DB with HP (LP or HP > DB). Error bars represent SEM, and the longest horizontal line represents the mean.

(A–D) The maximum height of the first paw raise of the stimulated paw in CD1 males (A), CD1 females (B), C57 males (C), and C57 females (D).

(E–H) The paw velocity of the first paw raise of the stimulated paw in CD1 males (E), CD1 females (F), C57 males (G), and C57 females (H).

(I–L) The pain score for a given animal to each stimulus in CD1 males (I), CD1 females (J), C57 males (K), and C57 females (L). The pain score is a composite measurement of orbital tightening, jumping, paw shaking, and paw guarding.

Genotype and sex are indicated at top of each column; n = 10 animals for all groups.
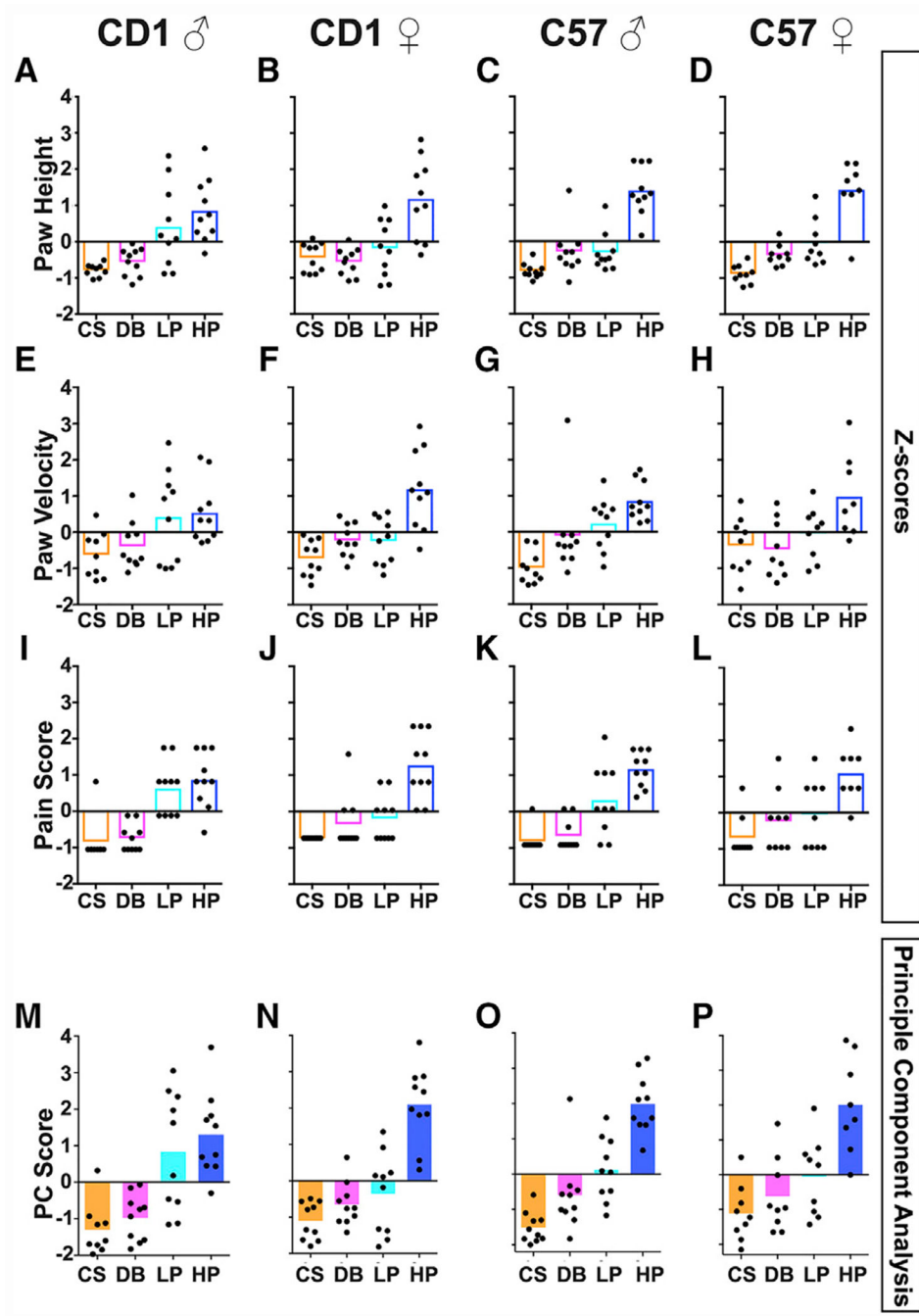
Figure 3. Statistical Analyses to Normalize the Three Parameters into One PC Score

(A–L) Z scores of individual mice are plotted relative to the combined mean from the four groups of sex and genotype in Figure 3. Each dot represents an individual mouse. Multiple trials of the same mouse from the same stimulus were averaged first for this analysis. Plotted are Z scores for paw height in CD1 males (A), CD1 females (B), C57 males (C), and C57 females (D); paw velocity in CD1 males (E), CD1 females (F), C57 males (G), C57 females (H); and pain score in CD1 males (I), CD1 females (J), C57 males (K), and C57 females (L). (M–P) The PC1 was plotted as a PC score following calculation of Z scores for individual

measures and obtaining eigenvalues for CD1 males (M), CD1 females (N), C57 males (O), and C57 females (P).

Genotype and sex are indicated at top of each column; n = 10 animals for all groups.
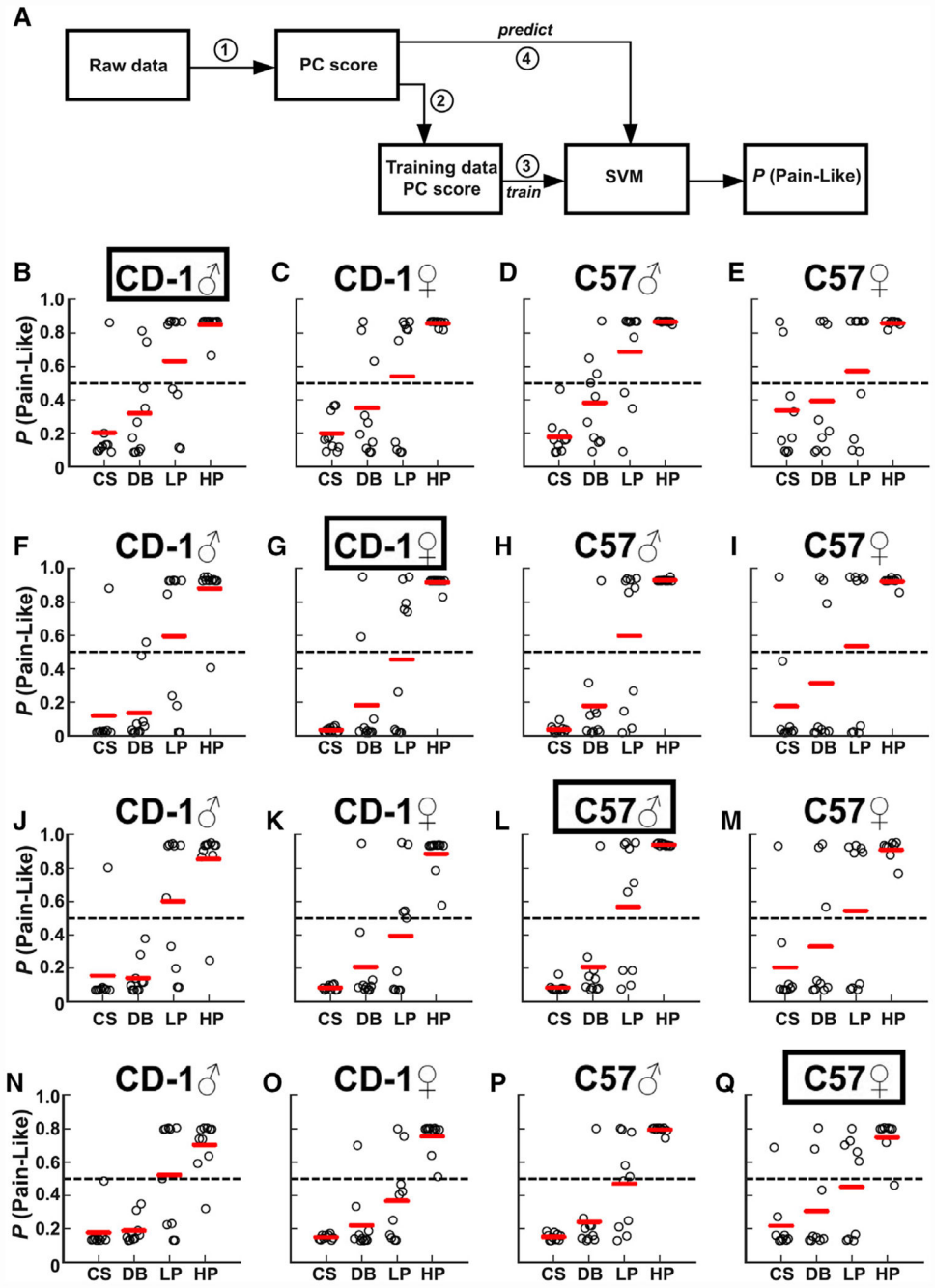
Figure 4. Machine Learning Predicts "Pain-like" Probability for Each Paw Withdrawal Reflex
A trained support vector machine (SVM) analyzed each behavior trial and output its probability of being pain-like.

(A) Graphical representation of the SVM process. Step (1): generate PCA1 eigenvalues from PCA datasets from Table 1. Step (2): calculate PC score of the PCA dataset. Step (3): train SVM with PC scores of fitting data (red circles). Step (4): predict pain-like probability (P [pain-like]) of all PC scores.

(B–E) Predictions made in CD1 males (B), CD1 females (C), C57 males (D), and C57 females (E) following training with CS and HP trials from CD1 males (outlined).

(F–I) Predictions made in CD1 males (F), CD1 females (G), C57 males (H), and C57 females (I) following training with CS and HP trials from CD1 females (outlined).

(J–M) Predictions made in CD1 males (J), CD1 females (K), C57 males (L), and C57 females (M) following training with CS and HP trials from C57 males (outlined).

(N–Q) Predictions made in CD1 males (N), CD1 females (O), C57 males (P), and C57 females (Q) following training with CS and HP trials from C57 females (outlined).
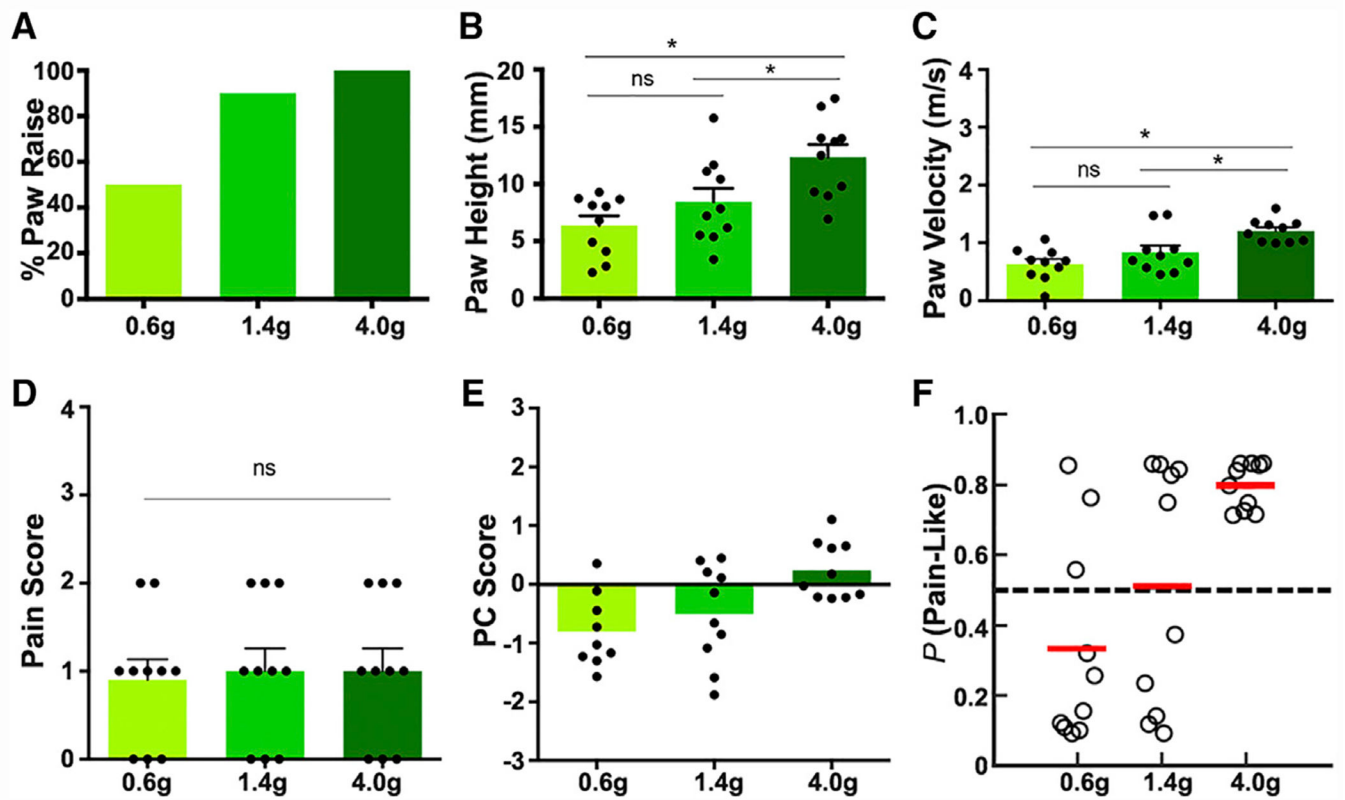
n = 10 animals for all groups.

Figure 5. Analysis of Mouse Paw Withdrawal Reflex in Response to von Frey Hairs
(A) Responsive rate of CD1 male mice to each VFH filament.

(B–D) Paw height (B), paw velocity (C), and pain score (D) were quantified for each VFH filament. Each dot represents an individual mouse.

(E) PC score plot for each VFH filament.

(F) SVM predications for each VFH filament. SVM was trained with CS and HP data of CD1 males.
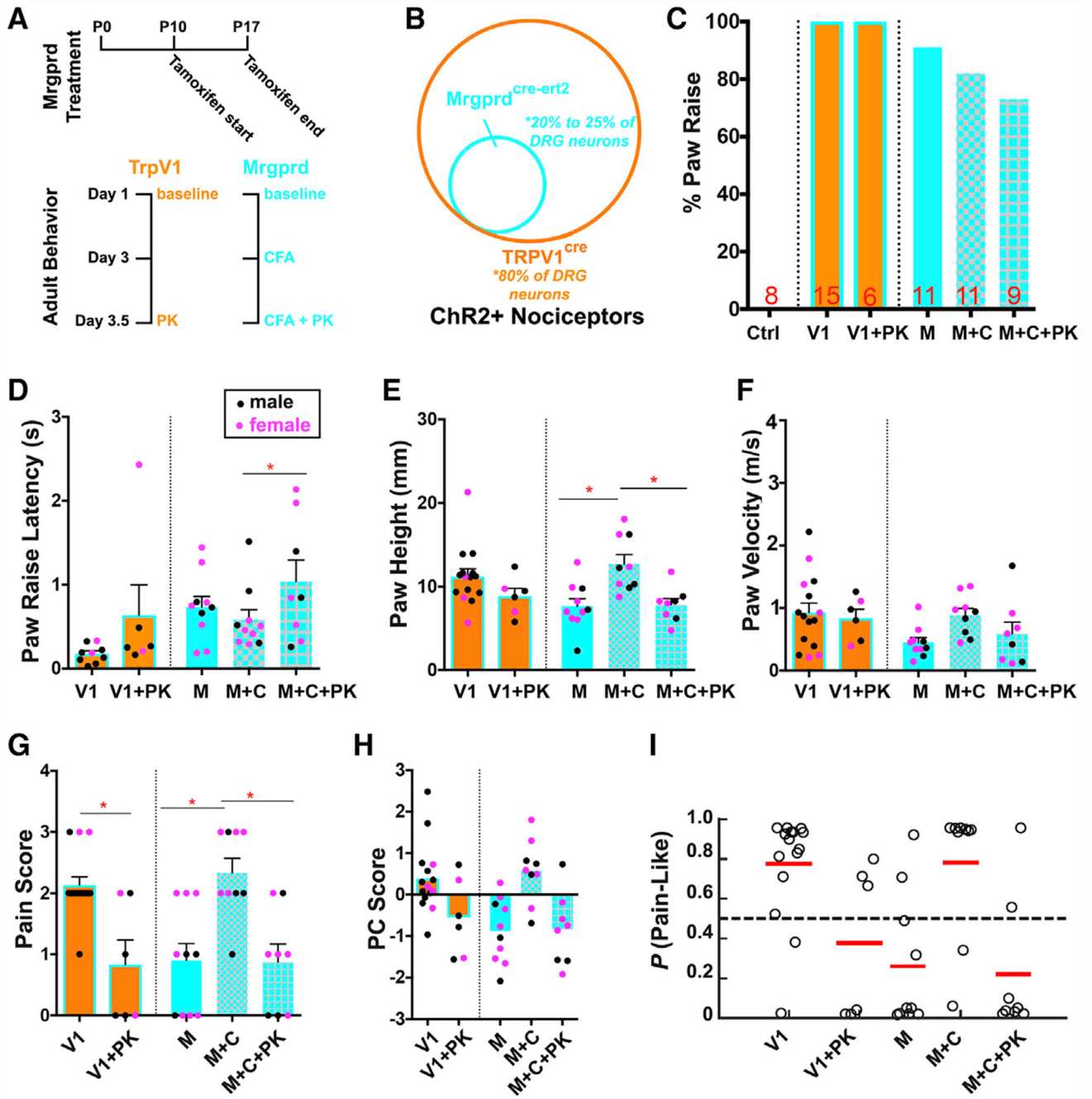
n = 10 animals for all groups.

Figure 6. Optogenetic Activation of TRPV1-ChR2+ and MRGPRD+ Primary Afferents

(A) Diagram of treatment paradigm and experimental design for paw reflexive behavior assays with *Trpv1-ChR2* mice (orange) and *Mrgprd-ChR2* (blue) mice.

(B) Graphical representation of the nociceptor populations targeted in *Trpv1-ChR2* and *Mrgprd-ChR2* mice.

(C) Percentage of animals displaying paw raise. "Ctrl" indicates *ChR2f/f* littermate control (n = 8 animals). "V" indicates *Trpv1-ChR2* mice at baseline (n = 15 animals), and "V+PK" indicates *Trpv1-ChR2* mice treated with painkiller (n = 6 animals). "M" indicates *Mrgprd-*

ChR2 mice at baseline (n = 11 animals), "M+C" indicates *Mrgprd-ChR2* mice at 3 days post-CFA (n = 11 animals), and "M+C+PK" indicates *Mrgprd-ChR2* mice receiving painkiller at 3.5 days after CFA injection (n = 9 animals).

(D) Latency between blue light stimulation and paw raise.

(E–G) quantification for paw height (E), paw velocity (F), and pain score (G).

(H) PC scores of *Trpv1-ChR2* and *Mrgprd-ChR2* mice at baseline, after CFA, and CFA + painkillers using eigenvectors derived from wild-type mice of both sexes and genotypes. Trials with female mice indicated as pink dots and males as black dots.

(I) SVM pain-probability graphs using all wild-type mice of both sexes and genotypes as training datasets to predict the probability of a pain response for *Trpv1-ChR2* and *Mrgprd-ChR2* optogenetic responses in baseline, after CFA, and CFA + painkillers.

Table 1.

PC Score and SVM Generation

Variable	C57 Male	C57 Female	CD1 Male	CD1 Female	C57+CD1 Female	C57+CD1 Male	Both Sexes + Strain
eigenvalues for first PC scores							
Z paw velocity	0.57742	0.58445	0.57431	0.59499	0.59098	0.56893	0.58267
Z paw height	0.60582	0.56067	0.59105	0.57074	0.56470	0.60710	0.58039
Z pain score	0.54731	0.58656	0.56641	0.56589	0.57605	0.55473	0.56888
fitting datasets for generating and training SVM							
Fitting datasets	C57(M) - CS,HP	C57(F) - CS,HP	CD1(M) - CS,HP	CD1(F) - CS,HP	na	na	CD1(M), CD1(F), C57(M), C57(F) - CS, HP
Figure	Figures 4I–4L	Figures 4M–4P	Figures 4A–4D and 5G	Figures 4E–4H	na	na	Figures 6I and 6J

Eigenvalues for calculating the PC1 scores are shown for each variable in each group of animals. These values were determined using SAS software using Data S2. The data used to generate and train the SVM to make predictions about pain-like probabilities for each group are also shown.

KEY RESOURCES TABLE

REAGENT or RESOURCE	SOURCE	IDENTIFIER
Antibodies		
chicken anti-GFP	Aves	GFP-1020; RRID:AB_10000240
rabbit anti-CGRP	Immunostar	24112; RRID:AB_2737130
conjugated IB4-Alex594	Molecular Probes	I21411; RRID:AB_2314662
guinea pig anti-VGLUT1	Fisher	AB5905; RRID:AB_2301751
rabbit anti-NFH	Sigma	N4142; RRID:AB_477272
rabbit anti-cFOS	Santa Cruz	sc-52; RRID:AB_2106783
Chemicals, Peptides, and Recombinant Proteins		
Complete Freud's Adjuvant	Sigma	F5881
Meloxicam	Penn Veterinary Hospital	N/A
buprenorphine	Henry Schein Animal Health	059122
Experimental Models: Organisms/Strains		
CD-1	Charles River	022; RRID:IMSR_CRL:22
C57BL6/J	Jackson Laboratory	000664; RRID:IMSR_JAX:000664
Mgprd^{CreERT2}	Jackson Laboratory	031286; RRID:IMSR_JAX:031286
ChR2 f/f	Jackson Laboratory	012569; RRID:IMSR_JAX:012569
TrpV1^{Cre}	Jackson Laboratory	017769; RRID:IMSR_JAX:017769
Pirt^{Cre}; GCAMP6(f)	Dong lab, Johns Hopkins University	N/A
Deposited Data		
Mendeley	This paper	https://data.mendeley.com/datasets/mcygb8762v/1
Github	This paper	https://github.com/longdecision/PainAssaySVM
Other		
473 nm blue laser light	Shanghai Laser and Optics Century	BL473T8-150FC/ADR-800A
10MHZ Function Waveform Generator	Agilent	33210A
FC/PC optogenetic patch cable	ThorLabs	M72L01
digital power meter	ThorLabs	PM100A
FastCAM UX100 high speed camera	Photron	800K-M-4GB
von Frey hairs	Stoelting Company	58011
concealer makeup brush	e.l.f™, CVS	N/A
Insect Pins	Austerlitz	N/A